

# Calcium oxalate monohydrate aggregation induced by aggregation of desialylated Tamm-Horsfall protein

Pragasam Viswanathan · Jeffrey D. Rimer ·  
Ann M. Kolbach · Michael D. Ward ·  
Jack G. Kleinman · Jeffrey A. Wesson

Received: 22 January 2010 / Accepted: 4 December 2010 / Published online: 13 January 2011  
© Springer-Verlag 2011

**Abstract** Tamm-Horsfall protein (THP) is thought to protect against calcium oxalate monohydrate (COM) stone formation by inhibiting COM aggregation. Several studies reported that stone formers produce THP with reduced levels of glycosylation, particularly sialic acid levels, which leads to reduced negative charge. In this study, normal THP was treated with neuraminidase to remove sialic acid residues, confirmed by an isoelectric point shift to higher pH. COM aggregation assays revealed that desialylated THP (ds-THP) promoted COM aggregation, while normal THP inhibited aggregation. The appearance of protein aggregates in solutions at ds-THP concentrations

$\geq 1$   $\mu\text{g/mL}$  in 150 mM NaCl correlated with COM aggregation promotion, implying that ds-THP aggregation induced COM aggregation. The aggregation-promoting effect of the ds-THP was independent of pH above its isoelectric point, but was substantially reduced at low ionic strength, where protein aggregation was much reduced. COM aggregation promotion was maximized at a ds-THP to COM mass ratio of  $\sim 0.025$ , which can be explained by a model wherein partial COM surface coverage by ds-THP aggregates promotes crystal aggregation by bridging opposing COM surfaces, whereas higher surface coverage leads to repulsion between adsorbed ds-THP aggregates. Thus, desialylation of THP apparently abrogates a normal defensive action of THP by inducing protein aggregation, and subsequently COM aggregation, a condition that favors kidney stone formation.

**Electronic supplementary material** The online version of this article (doi:10.1007/s00240-010-0353-7) contains supplementary material, which is available to authorized users.

P. Viswanathan · A. M. Kolbach · J. G. Kleinman ·  
J. A. Wesson (✉)  
The Nephrology Division of the Medical College of Wisconsin,  
Department of Veterans Affairs Medical Center, 111K,  
5000 West National Ave, Milwaukee 53295, WI, USA  
e-mail: jwesson@mcw.edu

J. D. Rimer · M. D. Ward (✉)  
Department of Chemistry, Molecular Design Institute,  
New York University, 100 Washington Ave, SE,  
New York, NY, USA  
e-mail: mdw3@nyu.edu

**Present Address:**  
P. Viswanathan  
Renal Research Lab, SBST, Center for Biomedical Research,  
VIT University, Vellore 632 014, Tamilnadu, India

**Present Address:**  
J. D. Rimer  
Department of Chemical and Biomolecular Engineering,  
University of Houston, 4800 Calhoun Ave.,  
S222 Engineering Bldg. 1, Houston, TX 77204, USA

**Keywords** Sialic acid · THP · Crystal aggregation ·  
Protein aggregation · Calcium oxalate · Kidney stone

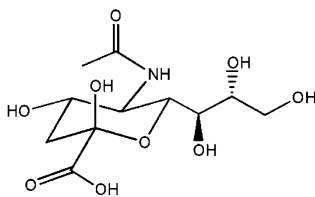
## Introduction

Kidney stone disease occurs in more than 10% of the US population, causing substantial suffering and occasional renal failure. The predominant component of most kidney stones is calcium oxalate monohydrate (COM). Stones are polycrystalline COM aggregates that form via four critical processes: nucleation, single crystal growth, aggregation, and attachment of crystals and/or aggregates to epithelial cells lining the distal nephron of the kidney [64]. Despite significant research efforts and clinical investigations of this disease during the last 50 years, adequate therapies and preventative drugs are lacking, revealing a compelling need for improved understanding of stone pathogenesis.

While nucleation and growth of stone crystals are essential processes in kidney stone formation, the evolution from crystals to clinical stones has been attributed in large part to the aggregation of pathological urinary crystals [13] potentially mediated through adhesion of urinary constituents to crystal surfaces. Indeed, recent investigations in our laboratories have linked adhesion events at calcium oxalate surfaces to differences in the pathological behavior of COM and calcium oxalate dihydrate (COD) [54]. Both stones and smaller crystalline aggregates retrieved from urine contain urinary macromolecules in the stone matrix, suggesting that macromolecules play a role in regulating stone formation [36, 47].

Differences in the ability of normal individuals and stone formers to retard or promote crystal aggregation have been attributed to macromolecules contained within their urine [43, 63]. Tamm-Horsfall protein (THP), a major component of stone matrix [6], exists in the terminal portions of the nephron and is the most abundant urinary protein produced in the kidney at  $\sim 100$  mg/day [60]. It is reasonable to suggest, therefore, that THP may play an important role in regulating stone formation. The primary structure of THP ( $\sim 85$  kDa) [21] contains 616 amino acids [37] with eight potential N-glycosylation sites. Although its role is generally thought to be protective [20, 35, 45, 50], some have suggested that THP can promote the formation of COM crystals and kidney stones [5, 18].

Desialylated proteins have been reported to reduce inhibitory activity of putative COM stone inhibitors, including prothrombin fragment-1 and osteopontin [28, 62]. Some investigators have reported reduced sialic acid contents in THP isolated from stone matrix [17, 30, 33, 52], while THP isolated from stone former urine has less sialic acid content than THP from healthy adults [26, 40]. This suggests that THP desialylation may be a risk factor for stone formation [66].



N-acetylneuraminic acid (NeuAc, "sialic acid")

Carboxylate groups of sialic acid contribute to the net anionic charge of THP, which influences intermolecular THP–THP interactions as well as protein adsorption on COM crystal surfaces [28, 29, 33, 61]. The role of native THP (n-THP) and desialylated THP (ds-THP) in the promotion and/or inhibition of both THP and COM aggregation has generated a degree of controversy. Disparities have been reported for the excretion rate of THP in urine [3, 14, 44], the THP sialic acid content in normal and stone

forming individuals [4, 16, 24, 26, 48, 56, 57], and the influence of THP concentration and sialic acid content in the promotion of COM stone formation [52]. Some of the confusion stems from the terminology used to describe stone formation as the promotion of "calcium oxalate (CaOx) crystallization" without specifying the crystalline form of CaOx (i.e., the monohydrate COM or dihydrate COD) or whether 'crystallization' refers to single crystal nucleation and growth or intercrystalline aggregation [20]. Comparisons often are made between *in vitro* experiments at different pH, ionic strength, and THP concentrations, which significantly influence COM aggregation [20, 32]. THP aggregates have been reported in several *in vitro* studies [1, 9–11, 23, 25, 31, 32, 38, 39, 50, 52, 55, 65], yet THP aggregates have not been observed in freshly voided urine of healthy individuals [16]. Some have suggested that THP precipitation may be a first step in stone formation [16, 18, 46], but the role of THP aggregates in regulating COM aggregation is not well understood.

To better elucidate the role of THP in stone formation, we have performed *in vitro* assays of both protein and crystal aggregation processes, including measurements of pH and ionic strength dependencies, specifically examining the differences between n-THP and ds-THP. At protein concentrations below  $8.4 \mu\text{g/mL}$ , n-THP did not self-associate into aggregates, whereas ds-THP formed  $1\text{-}\mu\text{m}$  sized aggregates at  $2 \mu\text{g/mL}$ , exhibiting monotonically increasing number density with increasing ds-THP concentration. The addition of n-THP to solutions of COM seeds did not promote COM aggregation, instead prompted disaggregation of pre-existing  $10\text{-}\mu\text{m}$  aggregates of individual COM crystals (so-called "COM seeds"). In contrast, ds-THP promoted COM aggregation, with maximum aggregation observed at an intermediate ds-THP concentration, which can be explained by ds-THP aggregates that bridge opposing crystal surfaces at partial surface coverage, but frustrate aggregation at higher coverage due to repulsive interactions between ds-THP aggregates on opposing crystal surfaces, which may involve electrostatic forces. This explanation is corroborated by a model based on  $1\text{-}\mu\text{m}$  spherical ds-THP aggregates and an adjustable ds-THP aggregate–COM surface equilibrium binding constant. Experimental observations and modeling collectively reveal that desialylation abrogates a normal defensive action of THP by inducing ds-THP aggregation, which subsequently promotes COM aggregation. This effect could increase the risk of kidney stone formation.

## Materials and methods

All purchased chemicals were of reagent grade and used without further purification. All solutions were prepared in

water that was purified (to 18 M $\Omega$  resistance) using the Nanopure II system (Barnstead, Boston, MA).

#### Urine collection

Urine was collected in the presence of an EDTA-free protease inhibitor cocktail (Roche Applied Science, Indianapolis, IN) from one individual without a personal or family history of kidney stones. The institutional review board and research committee of the institutional affiliations approved these studies.

#### Urine macromolecule mixture preparation

Urine macromolecules (UMs) were isolated by ultrafiltration (10 kDa MiniKros, Spectrum Laboratories, California) against 100 mM NaCl as previously described [63]. Macromolecular fractions were concentrated five to tenfold in the presence of protease inhibitors (Sigma, St. Louis, MO) and samples were stored at  $-80^{\circ}\text{C}$  until assayed.

#### Isolation and purification of THP

THP was isolated and purified as described previously [15, 51]. Briefly, urine was filtered through diatomaceous earth that was preconditioned by washing with deionized water followed by 0.25 M phosphate buffer containing 0.14 M NaCl. The diatomaceous earth was then suspended in 150 mL of water with continuous stirring for 30 min, followed by centrifugation (7,000 rpm, 30 min,  $4^{\circ}\text{C}$ ) to collect the supernatant. THP was isolated from the supernatant by increasing the ionic strength of the solution to 0.58 M NaCl and allowing 24 h for THP precipitation at  $4^{\circ}\text{C}$ . Centrifugation of the suspension containing THP precipitate resulted in the formation of a solid THP pellet that was dissolved in alkaline water (pH 9.0) overnight at  $4^{\circ}\text{C}$ . The resulting suspension was again precipitated by NaCl addition, isolated by centrifugation, and redispersed in 1 mL of deionized water containing 0.1 mM phenylmethyl sulfonyl fluoride (PMSF). Isolated THP, labeled native THP (n-THP), was analyzed by MALDI-TOF mass spectrometry at the Medical College of Wisconsin Protein and Nucleic Acid Facility to confirm the protein identity.

#### Protein quantification

Purified Tamm-Horsfall protein concentrations were determined using the BCA protein assay test kit (Pierce #23227), while the concentrations of isolated UMs were determined using a protein dye reagent (Biorad, 500-0006). Standard curves for absorbance as a function of protein concentration were generated for each test kit using serial dilutions of bovine serum albumin.

#### Desialylation of THP

Portions of n-THP (0.8–42  $\mu\text{g}/\text{mL}$ ) were desialylated using neuraminidase isolated from *Vibrio cholerae* (Sigma) in 10 mM sodium acetate buffer (pH 5.5) at  $37^{\circ}\text{C}$  for 24 h to produce desialylated THP (ds-THP-S). Alternatively, portions of n-THP were treated in a similar procedure using *V. cholerae* neuraminidase conjugated to agarose beads (Calbiochem, Los Angeles, CA). The agarose bead-conjugated neuraminidase was then removed from the supernatant by brief centrifugation, yielding desialylated THP (ds-THP-B) without residual neuraminidase enzymes present. Samples were stored at  $4^{\circ}\text{C}$  until further analysis.

#### Carbohydrate analysis on native and desialylated THP

Total carbohydrate content was determined using a glycoprotein carbohydrate estimation kit (Pierce, Rockford, IL). The glycoprotein was first oxidized with sodium meta-periodate to form aldehydes that reacted with the detecting reagent. The reaction was visually confirmed by the formation of a purple by-product and was quantified spectroscopically using an absorbance (550 nm) proportional to the carbohydrate content of the glycoprotein. Sialic acid content was determined using a SIALICQ kit (Sigma, St. Louis), where a known amount of THP was enzymatically hydrolyzed using *N*-acetylneuraminic acid aldolase and subsequent products were reduced to lactic acid by  $\beta$ -NADH and lactic dehydrogenase. The extent of  $\beta$ -NADH oxidation was determined from the change in absorbance at 340 nm.

#### Polyacrylamide gel electrophoresis

Polyacrylamide gel electrophoresis (PAGE) was performed using 4–12% NuPAGE gels at 200 V for 50 min (MOPS buffer, Invitrogen). Molecular weights of both n-THP and ds-THP were estimated with SeeBlue molecular weight standards (Invitrogen). Gels were stained using SYPRO Ruby stain (Molecular Probes), imaged by UV trans-illumination with a Kodak IS2000 MMT imaging system, and Kodak MI software was used for protein molecular weight and densitometry data analysis.

#### Western blots

PAGE gels were transferred to nitrocellulose membranes (0.2  $\mu\text{m}$ ) with a Transblot transfer cell (Biorad; 25 mM Tris base, 192 mM glycine, 20% methanol, pH 8.4). Ponceau S (0.3%) in 1% trichloroacetic acid was used as a general stain for blotted proteins. THP was incubated overnight with an anti-THP antibody prepared in our laboratory against human THP (rabbit polyclonal, 1:100,000),

followed by washing with Tris buffered saline (TBST, 0.5% Tween 20, pH 7.4) to remove non-specific THP binding, and subsequent incubation with goat anti-rabbit horseradish peroxidase antibody (1:5,000) for visualization. Chemiluminescent images were acquired (IS2000 MMT, Kodak) with a SuperSignal West Femto substrate (Pierce). Purified THP was used as a calibration standard for quantitative Western blots of THP content in UM.

#### Far Western blots

Concentrated urinary macromolecules (140 µg of total protein per gel, ~8 µg/lane) were run on a single-well gel and blotted as described in the PAGE methods. Blots were blocked for non-specific binding using skim milk (2% in TBST), incubated overnight with n-THP or ds-THP (25 µg/mL) using a manifold (Immunetics), and washed extensively (3×, TBST) for 10 min. The blots were probed with the same polyclonal anti-THP antibody (1:100,000) and processed analogous to Western blotting protocols, ensuring equal acquisition time frames for all chemiluminescent images. The primary antibody detected total THP, identifying individual and aggregated THP as well as THP complexed with other urinary proteins. Non-immune rabbit serum and anti-THP alone were run as negative and positive controls, respectively.

#### Isoelectric focusing on native and desialylated THP

Small quantities (2 µg) of n-THP or ds-THP-S were immobilized on 11-cm gradient strips (Ready strip IPG strips, pH 3–6, Bio-Rad), which were soaked overnight with protease and phosphatase inhibitors prior to isoelectric focusing (3,000 V for 9 h). The second dimension (2D) was performed on a Criterion 4–12% Bis Tris PAGE system using MOPS buffer (Biorad). The proteins were blotted to nitrocellulose and probed for the presence of THP with the same polyclonal anti-THP antibody and processed as described in Western blotting. Centroid band analysis was used to determine isoelectric point (pI) mobility shifts and intensity weight averages.

#### Calcium oxalate monohydrate crystal slurry

COM crystals, prepared as previously described [63], were analyzed by solid state IR (National Crystal ID Center, Milwaukee, WI) to confirm the synthesis of monohydrate crystals. Dried COM powders were dispersed in a slurry (1.5 mg/mL in HB; 150 mM NaCl; 10 mM HEPES, pH 7.5) at least 3 weeks prior to assays, yielding suspensions of COM seeds composed principally of crystal aggregates, with a weight average diameter of about 10 µm, as determined by particle sizing (described below).

#### COM aggregation assay

Equimolar calcium and oxalate solutions were used to conduct COM aggregation assays as reported earlier [63]. Solutions were assayed by particle sizing (see following section for details) in slightly supersaturated solutions,  $s = 1.11$ , where  $s = [\text{Ca}^{2+}]/[\text{Ca}^{2+}]_0$  and  $[\text{Ca}^{2+}]_0$  is the equilibrium concentration, or solubility, determined empirically as the concentration at which the COM seeds neither increased nor decreased in size after 1 h of stirring in control solutions. A slightly supersaturated reaction condition was chosen to prevent COM dissolution, such that the observed changes in COM seed size were predominantly associated with aggregation. Briefly, 300 µg of COM seed crystal was added as an aqueous suspension at equilibrium to a 5-mL reaction volume containing either n-THP, ds-THP, or no added protein (control). After stirring for 1 h at 37°C, an aliquot was dispersed in sizing buffer ( $s = 1.0$ ) for particle size determination. Various concentrations of THP and ds-THP were used in aggregation studies, up to a maximum protein concentration of 8.4 µg/mL, which is below the THP concentration typically found in urine [27, 42]. Experiments were performed at pH 7.5 in solutions with high ionic strength (150 mM NaCl, 10 mM HEPES) and low ionic strength (i.e., no added NaCl). A 0.1 M sodium acetate buffer was used to reduce solution alkalinity for analyses at pH 5.5 and similar ionic strengths. Table 1 lists equilibrium concentrations measured for each experimental condition.

#### Particle size distribution analysis

Particle sizing, measured with an Accusizer 780/SIS (Particle Sizing Systems, Santa Barbara, CA), was used to detect THP aggregation and to assess the extent of COM crystal aggregation. This instrument is sensitive to particle size within the size range of 0.5–400 µm diameters. PSDs were measured immediately in solutions containing 15 µg COM in 15 mL of sizing buffer (150 mM NaCl, 10 mM HEPES, 0.22 mM CaCl<sub>2</sub>, and 0.22 mM Na<sub>2</sub>C<sub>2</sub>O<sub>4</sub>). PSDs are reported as the average of three or more replicated experiments. Aggregation data from PSD analyses are

**Table 1** Equilibrium concentrations of COM in various buffer conditions (based on interpolation, uncertainty ±0.01 mM)

Experimental condition	$[\text{Ca}^{2+}]_0$ (mM); $s = 1^*$
150 mM NaCl, pH 7.5*	0.22
No salt, pH 7.5	0.10
150 mM NaCl, pH 5.5	0.18
No salt, pH 5.5	0.09

\* COM aggregation sizing buffer assay conditions,  $s = [\text{Ca}^{2+}]/[\text{Ca}^{2+}]_0$

reported as  $R_D$ , where  $R_D = D_f/D_0$ ,  $D_f$  is the weight-averaged particle diameter measured after 1 h, and  $D_0$  is the initial weight-averaged particle diameter of the COM “seeds” (time = 0).

#### Zeta potential ( $\zeta$ ) measurements of n-THP and ds-THP

Protein zeta potentials ( $\zeta$ ) were measured with a NICOMP 380/ZLS instrument (Particle Sizing Systems, Santa Barbara, CA) using 4-mL polymethacrylate cuvettes (Fisher Scientific, Chicago, IL) filled with a total volume of 3 mL. Approximately, 750  $\mu\text{g}$  of COM crystal was added as an aqueous suspension at equilibrium ( $s = 1.0$ ) to a sample cuvette containing saturated calcium oxalate solution in NaCl buffer followed by the addition of either n-THP or ds-THP-S at 1.6  $\mu\text{g}/\text{mL}$ , allowing 1 h of equilibration prior to zeta potential measurement. The uncertainty in  $\zeta$  was estimated as  $\pm 2$  mV based on repeated measurements.

#### Statistical analysis

All measured values are expressed as  $M \pm SD$  ( $M$  = mean,  $SD$  = one standard deviation), where a Student's  $t$  test was used to determine statistical significance (defined in the usual manner as probability,  $p < 0.05$ ).

## Results

#### Protein characterization

The amount of THP isolated from a healthy individual was determined from Western blots of three separate random urine collections (see Supporting Information), which were normalized to creatinine concentrations in urine to facilitate comparison to published data. Concentrations of purified n-THP were obtained from calibration curves, plotting optical density (in pixels) versus quantity of loaded THP (in ng). The mean THP excretion rate from three collections was  $10 \pm 3$   $\mu\text{g}$  THP/mg creatinine, consistent with previous reports of THP content in normal urine determined by direct ELISA [27, 42]. The sialic acid content of n-THP was  $52 \pm 2$   $\mu\text{g}/\text{mg}$ , which was similar to values reported by others [24, 26, 56]. THP desialylation with soluble neuraminidase enzyme (ds-THP-S) reduced total carbohydrate content by 50% and reduced sialic acid content by approximately 40% ( $32 \pm 4$   $\mu\text{g}/\text{mg}$  ds-THP-S) relative to n-THP. Desialylation with the bead bound neuraminidase enzyme (ds-THP-B) reduced sialic acid content by 25% ( $39 \pm 2$   $\mu\text{g}/\text{mg}$ ), but the total carbohydrate content could not be determined due to the limited supply of protein available. Additional removal of THP sialic acid was not performed, since removing the remaining residues

required longer neuraminidase reaction times that resulted in degradation of THP, as evidenced by changes in band position in PAGE analysis. Nonetheless, the amounts of sialic acid in ds-THP-S and ds-THP-B used in these studies were similar to and only slightly higher, respectively, than values reported for THP samples isolated from stone formers [26, 40]. Consequently, these samples provide reasonable in vitro models for naturally occurring sialic acid content in THP.

The molecular weight of THP was determined by standard PAGE (see Supporting Information), in which the polyclonal antibody raised against human THP was insensitive to changes in sialic acid content. These gels exhibited no evidence of THP degradation, fragmentation, or aggregation. The molecular weights of n-THP, ds-THP-B, and ds-THP-S were measured as 80.5, 80.0, and 79.6 kDa, respectively. Small variations in molecular weight are attributed to mass loss from THP desialylation (i.e., removal of carbohydrate and sialic acid residues), but they also may reflect changes in THP charge/mass ratio, which affects protein mobility in PAGE analyses.

The isoelectric point (pI) of n-THP and ds-THP-S were determined using 2-D gel electrophoresis (Fig. 1). Densitometry tracings were measured for each of the bands evident in the Western blot (upper, inset), assuming a linear pH gradient for gels over the range  $3 < \text{pH} < 6$ . Heterogeneity in the number of residual glycosylation sites among individual proteins results in a range of pI values, in which n-THP exhibits a more acidic pI range (3.2–4.3) than ds-THP-S (4.0–5.0), consistent with fewer negatively charged sialic acid groups on ds-THP-S. The upper pI limit of the ds-THP-S band corresponds reasonably well to the pI value of 5.05 predicted for the unmodified amino acid backbone [58]. The weight average pI values for n-THP and ds-THP-S

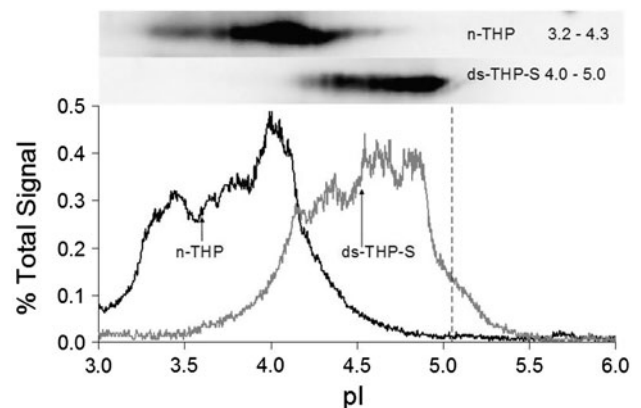


**Fig. 1** 2D Western blot of n-THP and ds-THP. THP (2  $\mu\text{g}$ ) was focused on a 3–6 immobilized linear pH gradient. Signal intensity profiles are shown as a percentage of the total pixel across the centroid of the protein band. The predicted isoelectric point of THP based on the amino acid backbone is shown as a vertical dashed line

were 3.9 and 4.5, respectively. The difference in these two values is similar to those reported for n-THP and stone-former THP [49], as measured by isoelectric focusing with one-dimensional gel electrophoresis using a non-specific protein stain rather than a specific THP antibody, and thus did not exclude contributions from other proteins.

### Crystal aggregation

The effects of pH, ionic strength, and THP concentration on COM crystal aggregation were examined by particle size analysis of 5-mL buffer solutions containing 300  $\mu\text{g}$  of COM “seeds”. The degree of aggregation promotion was surmised from the net change in seed size, characterized as  $R_D = D_f/D_0$ , where  $D_f$  is the weight-averaged diameter measured after 1 h and  $D_0$  is the initial weight-averaged diameter of the COM seeds (time = 0). The effects of pH and ionic strength were examined in a  $2 \times 2$  experimental matrix defined by pH = 5.5 or 7.5 and no NaCl or 150 mM NaCl in supersaturated solutions of calcium oxalate ( $s = 1.11$  for  $[\text{Ca}^{2+}]$  and  $[\text{Ox}^{2-}]$ ) for a THP concentration of 1  $\mu\text{g}/\text{mL}$  (see Fig. 2). The pH values in these studies were chosen to be near the upper and lower bounds of urine pH (i.e., pH 5–8). Notably, physiological pH is higher than the average pI values of THP (n-THP = 3.9, ds-THP = 4.5; vide infra); consequently, the proteins can be expected to have some anionic character (i.e., deprotonated carboxylate groups). Under all four conditions, solutions containing n-THP showed a significant reduction in COM particle size ( $R_D < 1$ ) with negligible differences between the pH and ionic strength conditions tested, indicating that n-THP was capable of disrupting pre-existing COM aggregates, an effect that can be described as disaggregation [63]. Conversely, ds-THP-S promoted COM aggregation ( $R_D = 2.0$ ) at both high ionic strength conditions (150 mM NaCl), but demonstrated no significant difference from control at low ionic strength (no added NaCl). The effect of ds-THP-S on COM aggregation was apparently independent of pH, similar to results for n-THP.

The effects of n-THP and ds-THP on COM crystal aggregation were examined at various protein concentrations (0.16–8.4  $\mu\text{g}/\text{mL}$ ) mixed with 300  $\mu\text{g}$  of COM in 5 mL of the standard buffer (pH 7.5, 150 mM NaCl, 10 mM HEPES). Disaggregation of COM seeds was observed for all n-THP solutions, while both ds-THP-S and ds-THP-B promoted COM aggregation ( $R_D > 1$ ), with ds-THP-S exhibiting maximum aggregation promotion at a protein/COM mass ratio (MR) of  $\sim 0.025$  (Fig. 3a). Aggregation was less pronounced for ds-THP-B, which was likely attributable to its higher sialic acid content relative to ds-THP-S. As indicated in [Materials and methods](#), the amounts of available ds-THP-B were insufficient to perform studies across the full range of MR

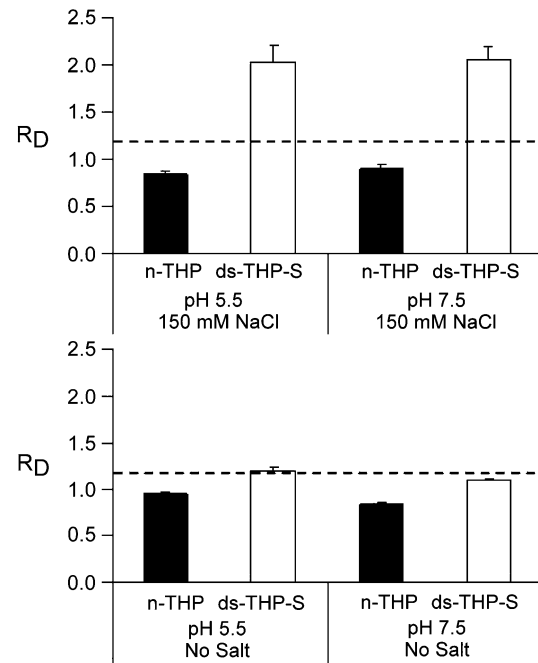


**Fig. 2** COM aggregation induced by THP (1  $\mu\text{g}/\text{mL}$ ) at various pH and ionic strength values. *Upper panel* experimental conditions at 150 mM NaCl and at pH 5.5 and 7.5. *Lower panel* experimental conditions with no added salt and at pH 5.5 and 7.5. The n-THP data are labeled as *solid bars*, the ds-THP-S data as *open bars*, and the *dashed lines* correspond to the average COM aggregation control ( $R_D = 1.03 \pm 0.04$ )

values in Fig. 3a, which otherwise may have revealed a maximum value of  $R_D$  at a specific mass ratio. The behavior of ds-THP-S was reinforced by PSD measurements of  $R_D$  in which the MR was adjusted by varying the COM mass content from 0.037 to 3.0 mg while maintaining the ds-THP-S concentration at a fixed value of 4.2  $\mu\text{g}/\text{mL}$ . A maximum was observed at nearly the same MR value as in the measurements performed with a fixed COM mass with varying protein concentrations (also see Fig. 6). Samples of ds-THP-S contained trace amounts of neuraminidase enzyme remaining from desialylation, but a solution containing 5 nM neuraminidase enzyme only (equal to the concentration in ds-THP-S) revealed minimal disaggregation of COM seeds (Enzyme Control, EC in Fig. 3a). This observation and the ds-THP-B data together indicate that the presence of neuraminidase did not contribute to the aggregation promotion observed in ds-THP-S samples.

### Protein aggregation

Particle size measurements of ds-THP-S solutions, performed in the absence of COM, revealed a monotonic increase in the number of particles with increasing concentration (Fig. 3b), relative to the background for the

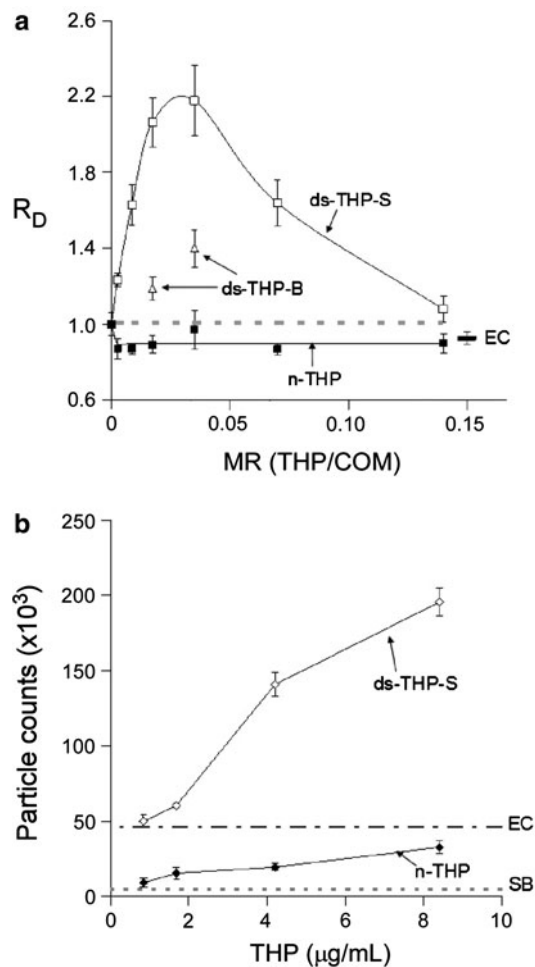


**Fig. 3** **a** Upper panel COM aggregation with n-THP and ds-THP, plotted as changes in COM seed diameter ratio,  $R_D$ , with increasing THP/COM mass ratio, MR, for solutions at constant COM concentration (60  $\mu\text{g/mL}$ ) and varying THP content (0–10  $\mu\text{g/mL}$ ). All points are significantly different from control (gray dashed line) except the 2  $\mu\text{g/mL}$  concentration for n-THP. In general, the n-THP (filled squares) samples tested yielded  $R_D$  less than control (indicating disaggregation), while ds-THP-S (open squares) significantly promoted COM aggregation at all concentrations, indicated by  $R_D > 1$ . Moderate aggregation promotion was noted in ds-THP-B (triangles) samples, where only two data points were assayed due to the limited quantity of protein available. Neuraminidase tested at assay concentrations had a slight disaggregating effect (EC). **b** Lower panel particle counts of the protein samples without COM seed crystal added. Native THP (filled diamond) had particle counts slightly greater than the sizing buffer (SB), while ds-THP-S (open diamond) revealed an increasingly large number of particles with increasing ds-THP-S concentration, and all were significantly greater than the neuraminidase control (EC)

neuraminidase control, which can be attributed to ds-THP-S aggregate formation. The change in particle size with concentration was negligible, suggesting that the protein aggregates achieved a characteristic size, but grew no larger (although most particles had sizes near the lower limit of detection for this instrument). Parallel measurements of

n-THP solutions revealed substantially smaller particle counts ( $<EC$  at all points), suggesting the absence of protein aggregates in n-THP solutions. The appropriate background particle counts for n-THP solutions, however, must be gleaned from the sizing buffer (SB in Fig. 3). Given the low number of excess particles detected and the weak dependence on n-THP concentration, the possibility of a small amount of aggregate formation in this sample cannot be excluded, though it clearly is reduced substantially compared with ds-THP-S. Therefore, the data in Fig. 3b clearly indicate that d-THP-S aggregates much more extensively than n-THP, which likely remains predominantly in a molecularly dispersed form.

The aggregation of ds-THP at physiologic salt concentrations clearly correlates with promotion of COM aggregation, in vitro, implicating ds-THP aggregates in stone formation. The situation in the urine is complicated, however, by the presence of other proteins that also may interact with THP, COM surfaces, or both, and could further alter the effect of THP on crystallization processes and stone formation. One important aspect of these possible interactions, the propensity of THP to associate with other urinary proteins, has been explored by Far Western blotting. In Far Western blotting, urinary macromolecules, first separated by size in PAGE and blotted to nitrocellulose, are incubated in the presence of either n-THP or ds-THP-S, and then incubated with anti-THP to label all areas where ds-THP or n-THP are bound, thus identifying proteins that bind either THP form.

As shown in Fig. 4, incubating the blot of normal human urinary macromolecules with anti-THP resulted in a single, strong primary band detected at 80 kDa (lane 2, labeled  $\alpha$ -THP, Fig. 4), out of the many bands identified using Ponceau-S (PS, a general protein stain) of an identically prepared gel (lane 5, Fig. 4). Exposure of another identical blot to n-THP followed by anti-THP incubation yielded a weaker primary band at the same 80 kDa position, and little evidence of association with other urinary proteins (lane 3, Fig. 4). Incubation of another identical blot with ds-THP-S followed by incubation with anti-THP, however, revealed at least three intense bands at molecular weights of 61, 52, and 26 kDa, indicating strong associations of ds-THP with at least three other proteins. Bands with less intensity were identified at 72, 56, and 43 kDa, indicating additional, albeit weaker, associations with at least three additional urinary proteins (lane 4, Fig. 4). Identical results were obtained at four separate protein concentrations of n-THP and ds-THP-S spanning the range from 1 to 50  $\mu\text{g/mL}$ , except for the expected increased intensity of labeling with higher concentrations added. Bands were evident at each of these positions in the gel labeled with PS, indicating that these proteins were present in relatively high abundance in normal urine. The 61-kDa band was

likely albumin and the 26-kDa band was likely Ig-kappa, based on molecular weight markers (lane 1, Fig. 4) and relative abundance in urine, as well as the positive staining in Western blots from similar gels with specific antibodies. Band assignments are supported by earlier reports implicating serum proteins in urine, such as albumin, as promoters of THP aggregation [22], and by the observation that THP associates with other proteins (e.g., IgG light chains or Bence Jones protein) in renal cast formation [23, 39]. Based on the observation of the large number of associations between ds-THP and other urinary macromolecules, we anticipate that ds-THP aggregates formed during phase separation would trap many other proteins, which could foster stone formation by potentially altering the aggregate interactions with crystal surfaces or depleting the solution of molecularly dispersed proteins that serve as aggregation inhibitors.

#### Surface charge measurements

Since surface charge is an important factor stabilizing particles against aggregation, the crystal and protein surface charges were measured by zeta potential ( $\zeta$ , mV) measurements of solutions containing n-THP, ds-THP-S, and COM seeds, along with mixtures of each protein with COM crystals. COM seeds suspended in solutions at physiological pH without added protein had negatively charged surfaces ( $\zeta = -14$  mV). Incubation of seeds with 1.6  $\mu\text{g}/\text{mL}$  of either n-THP or ds-THP-S reduced the  $\zeta$

value to  $-8$  and  $-4$  mV, respectively, consistent with protein adsorbed on the COM crystal surfaces. The  $\zeta$  values of COM seeds with adsorbed proteins were nearly identical to those measured for corresponding proteins without COM ( $\zeta_{\text{n-THP}} = -6$  mV and  $\zeta_{\text{ds-THP-S}} = -4$  mV), suggesting that the adsorbed protein determines the surface charge. It should be noted that zeta potentials were calculated from electrophoretic mobility measurements, using light scattering to monitor particle diffusion under an applied electric field. In samples containing both COM and protein, the light scattering signal attributable to unbound protein in solution was negligible compared to the COM signal, and cannot explain the observed change in COM electrophoretic mobility.

#### Molecular model for THP-induced COM aggregation

A simple model describing the crystal aggregation observations above was developed using basic principles from polyelectrolyte theory to explain the differences in protein aggregation behavior exhibited by n-THP and ds-THP, coupled with a simple surface coverage model to explain the complicated concentration dependence of COM aggregation promotion on ds-THP aggregate concentration. This model describes all of the significant observations, including the initial increase and subsequent decrease in COM aggregate formation with increasing ds-THP concentration, the strong dependence of ds-THP-induced COM aggregation on salt concentration, and the negligible effect of pH on aggregate formation. Full details of the model are given in the Supplementary Materials, but the key features are enumerated here.

THP must be modeled as a partially charged polyelectrolyte chain. The peptide backbone of THP (excluding glycosylation) contains approximately 11% anionic amino acids (6% aspartic acid and 5% glutamic acid) [58], with only a few cationic residues (lysine and arginine), equivalent to a polymer with net negative charge and >85% hydrophobic amino acids. The number of anionic charges in n-THP can nearly double by adding branched N-glycan side chains that are rich in sialic acid groups to the eight possible sites on the protein backbone. Consequently, both n-THP and ds-THP have a relatively low net negative charge, as evidenced by the low zeta potentials:  $\zeta = -8$  and  $-4$  mV, respectively. For comparison,  $\zeta = -33$  and  $-24$  mV for poly(acrylate) and poly(aspartate), respectively. Polyelectrolyte aggregation, or phase separation, occurs when the number of charged groups per chain is insufficient to offset intermolecular hydrophobic interactions, resulting in the formation of polymer aggregates, in this case with a characteristic size reflecting the balance between exposing charged groups to water and hiding hydrophobic portions of the protein in the interior, similar

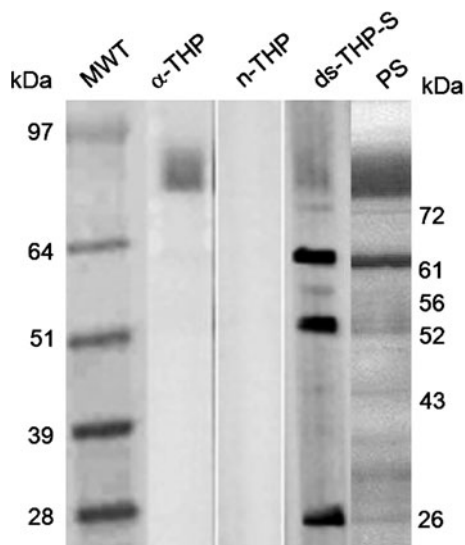


**Fig. 4** Far Western blots of urine macromolecules (UM) with n-THP or ds-THP. Lane 1 molecular weight markers, lane 2 anti-THP Western blot, lane 3 Far Western blot with n-THP (25  $\mu\text{g}/\text{mL}$ ) and lane 4 Far Western blot with ds-THP (25  $\mu\text{g}/\text{mL}$ ), lane 5 ponceau S (PS) total protein stain of UM prior to Western/Far Western blotting. Non-immune serum was run as a negative control (data not shown)

to interactions in micelle self-assembly. Increases in ionic strength via addition of NaCl will decrease protein solubility in water significantly by reducing the repulsive electrostatic forces stabilizing proteins in solution through charge screening, thereby promoting protein aggregation. The induction of weak polyelectrolyte aggregation by addition of salt, commonly known as “salting out”, was exploited in the isolation and purification of n-THP from urine, though at much higher NaCl concentrations than physiologic. Because of its lower net charge, ds-THP will become aggregated (phase separated) at a lower salt concentration than n-THP, explaining our observations at physiologic salt concentrations. Reducing pH also could favor THP aggregation due to the reduction in overall anionic charge through increased protonation of carboxylate groups, although this effect would be significant only when the pH is near or below the pKa of the carboxylate residues (i.e., pKa ~4, which is generally outside the range of normal urine pH).

The role of aggregate surface coverage of COM controlling crystal aggregation promotion was explored using an “aggregate binding model” that assumed equilibrium binding between non-deformable, spherical ds-THP aggregates with a 1- $\mu\text{m}$  diameter (consistent with the particle sizing measurements) and COM crystal surfaces (Fig. 5). The model also assumes that the crystal surface area occupied by protein aggregate particles is the sum of their cross-sectional areas, as determined from a mean diameter, independent of any specific aggregate packing arrangement on the surface. Any contribution to crystal aggregation from surface charge changes was ignored on the basis that the difference between the  $\zeta$  values for COM with adsorbed n-THP and adsorbed ds-THP was very small, coupled with the observation of  $\zeta$  values that were much lower in both cases than that measured for COM alone in simple ionic solutions. The model invokes COM aggregation driven by ds-THP aggregates that serve as adhesive bridges between opposing COM surfaces in which the aggregates bind directly to the crystal surfaces (e.g., carboxylate groups on the exterior surfaces of the aggregates binding to calcium ions on the crystal surface) rather than to each other. Based on the experimental data, molecularly dispersed proteins (i.e., n-THP) are presumed to be ineffective in forming adhesive bridges, either because they are too small to span the gap between crystals or because they do not associate with each other, thus precluding adhesion of opposing COM surfaces coated with n-THP. The fact that ds-THP forms protein aggregates with a characteristic size suggests that the protein aggregates do not adhere to each other, such that a bridge will not form between adjacent COM surfaces that are both coated with ds-THP aggregates. Because ds-THP aggregate formation substantially depletes the solution of molecularly

dispersed ds-THP, any competition for COM binding sites from molecularly dispersed ds-THP was ignored in this model. Note that for molecularly dispersed THP, sufficient protein was present in these suspensions to coat the available COM surface with thicknesses ranging from 3 to 500 layers for the MR values tested, assuming adsorption of THP was complete.

A more detailed examination of the model is required to fully explain the concentration dependence of COM aggregation on MR, including the rise and subsequent fall of  $R_D$  with increasing MR, along with the subtle, but distinctive, differences in the curve shapes observed in Fig. 6 for two different concentration series. In the first series, variations in MR were generated by varying ds-THP concentration at constant COM mass density (fixed COM), while in the second series, the ds-THP concentration was held constant with varying COM mass density (fixed ds-THP). The critical parameters for this equilibrium model are defined by Eqs. 1 and 2,

$$dsTHP + COM \xrightleftharpoons{K} (dsTHP - COM) \quad (1)$$

$$K = \frac{[dsTHP - COM]_A}{[dsTHP]_A [COM]_A} = \frac{x}{([dsTHP]_{A,o} - x)([COM]_{A,o} - x)} \quad (2)$$

where  $K$  (units of  $\text{L}/\text{m}^2$ ) is the equilibrium constant, and  $[ds\text{-THP}]_{A,o}$  and  $[COM]_{A,o}$  denote the total concentration of ds-THP aggregates and COM, respectively, expressed in terms of surface area per unit volume ( $\text{m}^2/\text{L}$ ). The term  $x$ , which represents the concentration of adsorbed protein aggregates in  $\text{m}^2/\text{L}$ , corresponds to the fractional coverage of COM by ds-THP aggregates,  $\phi$ , defined by  $\phi = x/[COM]_{A,o}$ . While an idealized, ordered arrangement of protein aggregates on adjacent COM surfaces could maximize crystal aggregate–crystal binding interactions at a surface coverage,  $\phi = 0.5$ , as depicted in Fig. 5a, the arrangement of protein aggregates at partial surface coverage is more likely random, which would lead to some repulsive protein aggregate–protein aggregate interactions at  $\phi < 0.5$ , frustrating COM aggregate formation. The value of  $K = 113 \text{ L}/\text{m}^2$  can then be calculated by rewriting Eq. 2 in terms of  $K$ ,  $\phi$ , and MR, and solving that expression, while applying the constraint that  $\phi < 0.5$  over the MR range where  $R_D > 1.1$  for these experimental data. With the value of  $K$  fixed,  $\phi$  can then be calculated for both fixed COM and fixed ds-THP experiments at all MR values, as shown in Fig. 6. Changes in  $K$  shift the curves to higher or lower fractional coverage. For example, reducing  $K$  below  $113 \text{ L}/\text{m}^2$  decreases  $\phi$  for both sets of experimental conditions, and increases the separation between model curves, but yields the same relationship between the calculated  $\phi$  values for the two different series at each value of MR. (See Supporting Information for full details.)

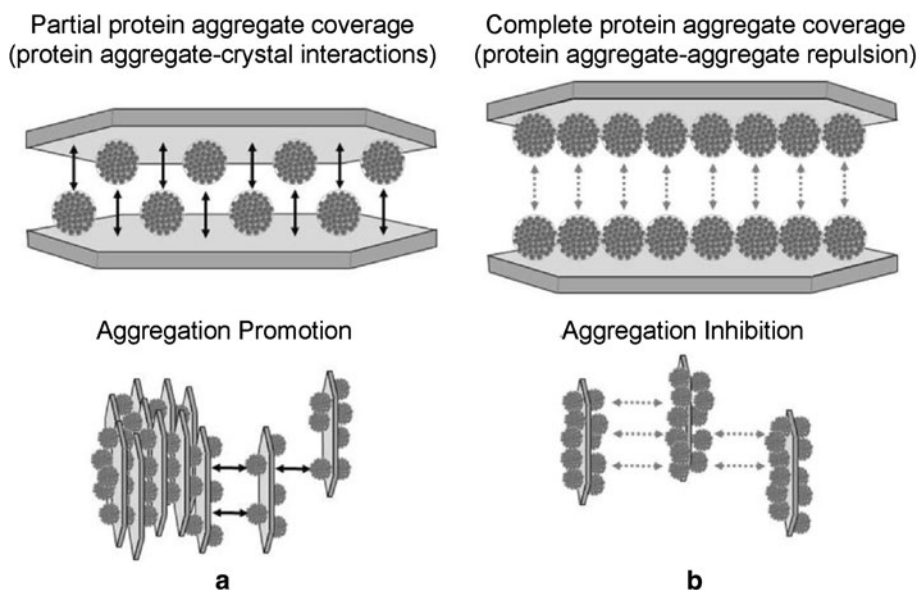


**Fig. 5** Diagram illustrating a proposed coverage dependency of ds-THP-COM aggregation. The COM “seed” surface is depicted as a single crystal for illustrative purposes, with the characteristic elongated hexagonal morphology of COM crystals. Adsorption is likely to occur on the (100) surface, which accounts for the largest surface area of single crystals, and is likely the predominantly surface area of COM seeds. Two cases are illustrated here for adsorption of aggregates to COM at (a) partial coverage (50%) and (b) complete

coverage (100%). The former promotes COM aggregation through crystal–protein–crystal bridging interactions, while at some threshold coverage (illustrated here as a surface completely covered with aggregates,  $\phi = 1$ ) repulsion between protein aggregates on opposing crystal surfaces offsets the attractive interactions resulting from any remaining crystal–protein–crystal bridges, leaving the crystals in a dispersed state

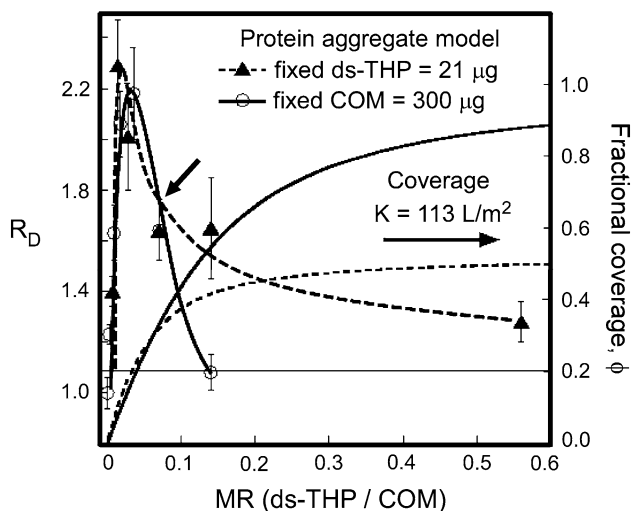


**Fig. 6** Equilibrium binding model analyses of protein adsorption on COM surfaces for ds-THP aggregates. Data are plotted as a function of ds-THP/COM mass ratio, MR, for fixed COM (300  $\mu\text{g}$ , circles, solid lines) and fixed ds-THP (21  $\mu\text{g}$ , triangles, dashed lines). Left axes change in COM seed diameter ratio,  $R_D$ , with error bars (one standard deviation) and interpolated lines drawn through data points. Measurements were obtained by light scattering using COM seeds ( $\sim 10 \mu\text{m}$  aggregates of individual crystals) suspended in 5 mL ds-THP solutions at various MR values. Right axes fractional surface coverage,  $\phi$ , of ds-THP aggregates on the COM surface (no symbols; solid line fixed COM; dashed line fixed ds-THP). The equilibrium binding constant  $K$  was adjusted to achieve  $\phi < 0.5$  at MR values where  $R_D > 1.1$ . See Supporting Information for details of model

Three observations are evident from the dependence of  $R_D$  on MR for fixed COM and fixed ds-THP conditions (Fig. 6). These features are most easily gleaned by starting from the point common to both data sets, indicated by the arrow, at  $R_D = 1.6$  and MR = 0.07 (21  $\mu\text{g}$  ds-THP and 300  $\mu\text{g}$  COM in the test solution). As MR increases from the reference point, there is a rapid decline in COM aggregate formation ( $R_D$ ) in the fixed COM series compared to a more gradual decline in the fixed ds-THP series. To the left of the reference point, the position of maximal  $R_D$  for the fixed ds-THP series occurs at a smaller MR value compared with the fixed COM series. Furthermore, there appeared to be a more rapid decline from the maximal  $R_D$  in the fixed ds-THP series, compared to the fixed COM series, though this difference is subtle. These observations are predicted from the equilibrium expression through the combined effects of reactant concentration and  $K$  on the fractional COM surface coverage by ds-THP aggregates. The model anticipates that at constant  $K$ , an increase in reactant concentration (combined [ds-THP] and [COM]) is accompanied by an increase in  $\phi$ . Each of the three observations noted above follows as a consequence.

The relationship between COM aggregation mediated by ds-THP and aggregate surface coverage can be illustrated by consideration of the right-hand side of Fig. 6, for MR > 0.07. For the fixed ds-THP series, MR was increased by reducing the COM concentration in the suspension.

Under this condition, the model predicts a very slow increase in  $\phi$  with increasing MR, eventually achieving a value of  $\phi \sim 0.5$  at  $MR = 0.6$ . The weak dependence of coverage on MR predicted by the model for  $MR > 0.07$  is consistent with the experimental observation of a very slow decline in  $R_D$  with increasing MR. For the fixed COM series, MR was increased by the addition of ds-THP to a suspension with a fixed quantity of COM; the model predicts that the surface coverage approaches  $\phi = 1$  at  $MR = 0.6$ . This condition corresponds to complete coverage of the COM surface with adsorbed aggregates, which prevents COM aggregation due to the absence of available contact surface for the adhesive aggregate bridges as well as repulsive interactions between adsorbed ds-THP aggregates on opposing COM surfaces.

The same principle operates in reverse as MR decreases from the reference point. In this circumstance, the MR decrease was accomplished by increasing COM concentration in the fixed ds-THP series or by decreasing ds-THP concentration in the fixed COM series. Starting from the reference point ( $\phi$  approximately 0.3), the fractional surface coverage falls more slowly in the fixed ds-THP series due to the higher total reactant concentration with decreasing MR (LeChatlier's principle), compared to the fixed COM series, as illustrated by the lines for  $\phi$  at lower MR values in Fig. 6. The maximal COM aggregation-promoting effect in the fixed ds-THP series, indicated by the maximum in  $R_D$ , clearly occurred at a lower MR value than the maximum  $R_D$  in the fixed COM series, as predicted from the model. As MR progresses toward 0,  $\phi$  continues to decrease, eliminating the aggregation-promoting effects and resulting in  $R_D$  falling rapidly to  $R_D = 1$  (no effect) in both series.  $R_D$  decreased more rapidly in the fixed COM series compared to the fixed ds-THP series due to lower  $\phi$  in the former, though the compression of the scale in this portion of Fig. 6 obscures the difference. Furthermore, the very low ds-THP concentrations required to reach these low MR values in the fixed COM series clearly approached the critical concentration for ds-THP aggregate formation, so a significant fraction of the ds-THP at the lowest MR conditions for the fixed COM series was likely in the molecularly dispersed form, further reducing aggregation-promoting effects. But, this additional factor was not included in the model.

## Discussion

The key observations from these experiments include (1) the demonstration of ds-THP protein aggregate formation, (2) the correlation between protein aggregate formation and COM crystal aggregation, and (3) the observation that maximal COM aggregation occurred only at a specific

proportion of THP to COM in the mixture. The latter was not anticipated on the basis of prior literature; however, the systematic approach to characterizing the association between THP aggregate formation and COM aggregation coupled with the understanding deriving from our model has created a context in which prior experimental results can be examined reliably for consistency. Many apparently discrepant observations from earlier publications related to the role of THP sialic acid content and solution conditions relevant to the urine environment, such as pH, ionic strength, and THP concentration [20], can now be explained on the basis of methodologic issues rather than by invoking unusual properties for specific patient samples. While many in vitro experiments have shown that adsorption of anionic urinary constituents on COM surfaces can modify promotion of crystal aggregation and crystal growth rates [8, 12, 13, 41, 53], these results illustrate the difficulty in designing experiments to distinguish urinary protein property differences between stone formers and healthy adults on the basis of crystal aggregation, and possibly other measures of protein effects on crystal formation (i.e., growth, nucleation or attachment), which are inherently indirect observations of protein-crystal surface interactions.

The critical property of THP related to its influence on COM aggregation is ultimately its solubility, which was directly correlated with sialic acid content in these experiments and inversely related to its propensity to self-aggregate. Several investigators have reported reduced sialic acid content in THP isolated from stone matrix [17, 30, 33, 52], which enhances the conversion of mucosubstances to mineralizable matrix in kidney stones [30]. Other studies have reported that THP isolated from stone former urine has lower sialic acid content than THP found in normal individuals [26, 40]. Increased sialidase activity in urine also is correlated with stone formation, which is suggestive of reduced sialic acid content on THP for those affected [59]. Furthermore, THP isolated from stone formers has been reported to contain a greater number of protein aggregates than THP from normal subjects, suggesting not only an alteration of the protein, but also a correlation between low sialic acid content and protein aggregation [4]. To our knowledge, only one contrary report [24] exists in which stone formers exhibit increased THP excretion with increased sialic acid content. Data from our experiments indirectly suggest a quantitative relationship between sialic acid content and protein aggregate formation through the reduced level of COM aggregation promotion exhibited by ds-THP-B (higher sialic acid content) compared with ds-THP-S (lower sialic acid content), illustrated in Fig. 4. Collectively, these observations support a relationship between decreased sialic acid content and stone formation as well as a

proclivity for THP to form aggregates, which has been described as a thermodynamic phase transition [32, 50].

Previous reports of the effects of THP on COM aggregation are somewhat conflicting. Many groups have investigated COM aggregation in the presence of both molecularly dispersed and aggregated THP without clearly identifying the role of protein aggregation in the promotion and/or inhibition of intercrystalline COM aggregation. As in this study, crystal aggregation promotion or loss of aggregation inhibition has been noted at conditions where aggregation of THP was presumed based on experimental conditions, but not determined definitively [2, 19, 20]. Others, however, have reported inhibition of COM aggregation at conditions where THP (with unspecified sialic acid content) remained molecularly dispersed in solution [19, 20, 50]. One report has asserted that desialylated THP favored aggregation of calcium oxalate crystals, whereas n-THP inhibited aggregation, though the state of THP aggregate formation was not assessed [17].

While previous reports suggested a link between the promotion of COM aggregation and THP aggregate formation under a variety of unique conditions, the most surprising result from the present study was the observation that high THP:COM mass ratios nearly eliminated aggregation promotion. This observation subsequently led to our model linking COM aggregation promotion to a fractional surface area coverage of COM by THP aggregate. The extent of aggregation promotion in either case (fixed COM concentration or fixed ds-THP concentration) increased with increasing ds-THP/COM mass ratio up to a maximum at MR  $\sim 0.025$ , followed by declining aggregation promotion as MR is increased further (Figs. 3a, 6). The model correctly predicts a slower decline for the fixed ds-THP series. Most previous reports have not controlled the THP:COM mass ratio in the manner described here. Consequently, COM aggregation behavior studied without control of the parameter could lead to a wide range of apparently inconsistent observations, from no observable effect to a doubling of COM aggregate size.

While the qualitative features of our model match our experimental observations for both fixed ds-THP and fixed COM conditions, thereby supporting the model, caution must be exercised when evaluating the model quantitatively. The ds-THP-S aggregate size ( $\sim 1 \mu\text{m}$  diameter) approaches the lower limit for our particle sizing instrument ( $0.5 \mu\text{m}$ ) and needs to be confirmed by other methods, (e.g., light scattering). The calculated COM crystal surface area covered by the aggregates depends on the square of their radius, and a small uncertainty in the protein aggregate size could affect the calculated surface coverage significantly. Moreover, the assumption of non-deformable aggregates, used to calculate the surface coverage, may not reflect the precise geometry of the aggregates when

adsorbed on the COM surface. These factors would affect the numerical value of the equilibrium constant, but not the general trends predicted by the model.

Finally, having identified the link between THP aggregate formation and COM aggregation promotion, the observations from the Far Western experiments that ds-THP associated with most major protein bands in a PAGE analysis of normal urine has important ramifications. Once THP aggregates begin to form, these results imply that most other urinary proteins will participate in that aggregation process, likely due to their essential similarity in molecular characteristics, specifically amphiphilic amino acid compositions (approximately, 80% hydrophobic and about 20% anionic amino acids). Consequently, many inhibitors of crystal aggregation may be bound up in THP aggregates, as well as proteins with strong COM affinities, which may either enhance protein aggregate binding to COM surfaces or deplete the solution of molecularly dispersed crystallization inhibitors. The observation of several dozen unique proteins in stone matrix, including many proteins not previously linked to crystallization or stone formation, is consistent with this proposed mechanism of crystal aggregate formation [7, 34].

In summary, the removal of sialic acid from THP lowers its anionic charge, thereby reducing its solubility and creating ds-THP aggregates through a phase separation process at physiologic saline concentrations, while n-THP remains molecularly dispersed at the same conditions. The formation of ds-THP aggregates correlated with the promotion of COM crystal aggregation, while the molecularly dispersed n-THP prevented COM crystal aggregation. Zeta potential and isoelectric point measurements revealed that n-THP was more negatively charged than ds-THP, consistent with expectations from the partially charged polyanion model. On the other hand, the difference in surface charge between the complexes formed by the two different THP forms with COM was small, suggesting repulsive electrostatic interactions were at most a minor contribution to inhibition of COM crystal aggregation. An aggregate binding model was developed, which predicts that partial coverage (10–20%) of COM crystal surfaces by ds-THP aggregates maximally promotes COM aggregation, while higher coverage frustrates aggregation, presumably due to repulsive aggregate–aggregate interactions between ds-THP aggregate layers adsorbed on opposing crystal surfaces. These investigations revealed that the physical structure of THP (i.e., molecularly dispersed vs. aggregated state), the relative concentration of ds-THP aggregates and COM, and the fractional coverage of adsorbed protein aggregates on the crystal surface are critical factors that determine whether THP promotes or inhibits COM aggregation in a given experiment. Experimental observations and modeling collectively reveal that aggregation

(phase separation) of ds-THP due to its reduced net charge abrogates the normal defensive action of molecularly dispersed n-THP—a result that qualitatively agrees with the previously observed link between reduced sialic acid content in THP and kidney stone formation. Furthermore, ds-THP demonstrated strong interactions with many other urinary proteins, potentially amplifying the deleterious effects of low sialic acid content THP in the process of stone formation.

**Acknowledgments** The authors thank Dr. Brian K. Olmsted for helpful discussions and Dr. William J. Zachowicz for performing the electrophoretic mobility (zeta potential) measurements reported in this study. This study was supported by the Veterans Affairs Merit Review Program (9305), the National Institutes of Health (NIDDK R01-DK068551), the Jacob Lemann Jr. Endowment Grant from the Medical College of Wisconsin, and the NYU Molecular Design Institute.

## References

- Bayer ME (1964) An electron microscope examination of urinary mucoprotein and its interaction with influenza virus. *J Cell Biol* 21:265–274
- Benkovic J, Furedi-Milhofer H, Hlady V, Cvorisec D, Stavljenic-Rukavina A (1995) Effect of Tamm-Horsfall protein on calcium oxalate precipitation. *Eur J Clin Chem Clin Biochem* 33:705–710
- Bichler K, Mittermuller B, Strohmaier WL, Feil G, Eipper E (1999) Excretion of Tamm-Horsfall protein in patients with uric acid stones. *Urol Int* 62:87–92
- Boeve ER, Cao LC, de Bruijn WC, Robertson WG, Romijn JC, Schroder FH (1994) Zeta potential distribution on calcium oxalate crystal and Tamm-Horsfall protein surface analyzed with Doppler electrophoretic light scattering. *J Urol* 152:531–536
- Boyce WH, King JS Jr (1963) Present concepts concerning the origin of matrix and stones. *Ann NY Acad Sci* 104:563–578
- Boyce WH, Swanson M (1955) Biocolloids of urine in health and in calculous disease. II. Electrophoretic and biochemical studies of a mucoprotein insoluble in molar sodium chloride. *J Clin Invest* 34:1581–1589
- Canales BK, Anderson L, Higgins L, Slaton J, Roberts KP, Liu N, Monga M (2008) Second prize: comprehensive proteomic analysis of human calcium oxalate monohydrate kidney stone matrix. *J Endourol* 22:1161–1167
- Cao LC, Deng G, Boeve ER, de Bruijn WC, de WR, Verkoelen CF, Romijn JC, Schroder FH (1996) Zeta potential measurement and particle size analysis for a better understanding of urinary inhibitors of calcium oxalate crystallization. *Scanning Microsc* 10:401–411
- Cavallone D, Malagolini N, Serafini-Cessi F (2001) Mechanism of release of urinary Tamm-Horsfall glycoprotein from the kidney GPI-anchored counterpart. *Biochem Biophys Res Commun* 280:110–114
- Clyne DH, Kant KS, Pesce AJ, Pollak VE (1979) Nephrotoxicity of low molecular weight serum proteins: physicochemical interactions between myoglobin, hemoglobin, Bence-Jones proteins and Tamm-Horsfall mucoprotein. *Curr Probl Clin Biochem* 9:299–308
- Clyne DH, Pesce AJ, Thompson RE (1979) Nephrotoxicity of Bence Jones proteins in the rat: importance of protein isoelectric point. *Kidney Int* 16:345–352
- De Yoreo JJ, Qiu SR, Hoyer JR (2006) Molecular modulation of calcium oxalate crystallization. *Am J Physiol Renal Physiol* 291:F1123–F1131
- Finlayson B (1978) Physicochemical aspects of urolithiasis. *Kidney Int* 13:344–360
- Ganter K, Bongartz D, Hesse A (1999) Tamm-Horsfall protein excretion and its relation to citrate in urine of stone-forming patients. *Urology* 53:492–495
- Gokhale JA, Glenton PA, Khan SR (1997) Biochemical and quantitative analysis of Tamm-Horsfall protein in rats. *Urol Res* 25:347–354
- Grover PK, Resnick MI (1995) Evidence for the presence of abnormal proteins in the urine of recurrent stone formers. *J Urol* 153:1716–1721
- Hallson PC, Choong SK, Kasidas GP, Samuell CT (1997) Effects of Tamm-Horsfall protein with normal and reduced sialic acid content upon the crystallization of calcium phosphate and calcium oxalate in human urine. *Br J Urol* 80:533–538
- Hallson PC, Rose GA (1979) Uromucoids and urinary stone formation. *Lancet* 1:1000–1002
- Hess B, Nakagawa Y, Coe FL (1989) Inhibition of calcium oxalate monohydrate crystal aggregation by urine proteins. *Am J Physiol* 257:F99–F106
- Hess B, Nakagawa Y, Parks JH, Coe FL (1991) Molecular abnormality of Tamm-Horsfall glycoprotein in calcium oxalate nephrolithiasis. *Am J Physiol* 260:F569–F578
- Hession C, Decker JM, Sherblom AP, Kumar S, Yue CC, Mattaliano RJ, Tizard R, Kawashima E, Schmeissner U, Heletky S (1987) Uromodulin (Tamm-Horsfall glycoprotein): a renal ligand for lymphokines. *Science* 237:1479–1484
- Hoyer JR, Seiler MW (1979) Pathophysiology of Tamm-Horsfall protein. *Kidney Int* 16:279–289
- Huang ZQ, Sanders PW (1995) Biochemical interaction between Tamm-Horsfall glycoprotein and Ig light chains in the pathogenesis of cast nephropathy. *Lab Invest* 73:810–817
- Jaggi M, Nakagawa Y, Zipperle L, Hess B (2007) Tamm-Horsfall protein in recurrent calcium kidney stone formers with positive family history: abnormalities in urinary excretion, molecular structure and function. *Urol Res* 35:55–62
- Jovine L, Qi H, Williams Z, Litscher E, Wassarman PM (2002) The ZP domain is a conserved module for polymerization of extracellular proteins. *Nat Cell Biol* 4:457–461
- Knorle R, Schnierle P, Koch A, Buchholz NP, Hering F, Seiler H, Ackermann T, Rutishauser G (1994) Tamm-Horsfall glycoprotein: role in inhibition and promotion of renal calcium oxalate stone formation studied with Fourier-transform infrared spectroscopy. *Clin Chem* 40:1739–1743
- Kobayashi K, Fukuoka S (2001) Conditions for solubilization of Tamm-Horsfall protein/uromodulin in human urine and establishment of a sensitive and accurate enzyme-linked immunosorbent assay (ELISA) method. *Arch Biochem Biophys* 388:113–120
- Konya E, Amasaki N, Umekawa T, Iguchi M, Kurita T (2002) Influence of urinary sialic acid on calcium oxalate crystal formation. *Urol Int* 68:281–285
- Lieske JC, Toback FG, Deganello S (2001) Sialic acid-containing glycoproteins on renal cells determine nucleation of calcium oxalate dihydrate crystals. *Kidney Int* 60:1784–1791
- Malek RS, Boyce WH (1973) Intraneuronic calculosis: its significance and relationship to matrix in nephrolithiasis. *J Urol* 109:551–555
- McQueen EG (1966) Composition of urinary casts. *Lancet* 1:397–398

32. McQueen EG, Engel GB (1966) Factors determining the aggregation of urinary mucoprotein. *J Clin Pathol* 19:392–396
33. Melick RA, Quelch KJ, Rhodes M (1980) The demonstration of sialic acid in kidney stone matrix. *Clin Sci (Lond)* 59:401–404
34. Merchant ML, Cummins TD, Wilkey DW, Salyer SA, Powell DW, Klein JB, Lederer ED (2008) Proteomic analysis of renal calculi indicates an important role for inflammatory processes in calcium stone formation. *Am J Physiol Renal Physiol* 295:F1254–F1258
35. Mo L, Liaw L, Evan AP, Sommer AJ, Lieske JC, Wu XR (2007) Renal calcinosis and stone formation in mice lacking osteopontin, Tamm-Horsfall protein, or both. *Am J Physiol Renal Physiol* 293:F1935–F1943
36. Nakagawa Y, Abram V, Parks JH, Lau HS, Kawooya JK, Coe FL (1985) Urine glycoprotein crystal growth inhibitors. Evidence for a molecular abnormality in calcium oxalate nephrolithiasis. *J Clin Invest* 76:1455–1462
37. Pennica D, Kohr WJ, Kuang WJ, Glaister D, Aggarwal BB, Chen EY, Goeddel DV (1987) Identification of human uromodulin as the Tamm-Horsfall urinary glycoprotein. *Science* 236:83–88
38. Porter KR, Tamm I (1955) Direct visualization of a mucoprotein component of urine. *J Biol Chem* 212:135–140
39. Prado MJ, Nicastrì AL, Costa PL, Rockman T, Tersariol IL, Nader HB, Barros RT, Prado EB (1997) The renal and hepatic distribution of Bence Jones proteins depends on glycosylation: a scintigraphic study in rats. *Braz J Med Biol Res* 30:865–872
40. Pragasam V, Kalaiselvi P, Subashini B, Sumitra K, Varalakshmi P (2005) Structural and functional modification of THP on nitration: comparison with stone formers THP. *Nephron Physiol* 99:28–34
41. Qiu SR, Wierzbicki A, Orme CA, Cody AM, Hoyer JR, Nancollas GH, Zepeda S, De Yoreo JJ (2004) Molecular modulation of calcium oxalate crystallization by osteopontin and citrate. *Proc Natl Acad Sci USA* 101:1811–1815
42. Reinhart HH, Obedeau N, Walz D, Sobel JD (1989) A new ELISA method for the rapid quantification of Tamm-Horsfall protein in urine. *Am J Clin Pathol* 92:199–205
43. Robertson WG, Peacock M (1972) Calcium oxalate crystalluria and inhibitors of crystallization in recurrent renal stone-formers. *Clin Sci* 43:499–506
44. Romero MC, Nocera S, Nesse AB (1997) Decreased Tamm-Horsfall protein in lithiasic patients. *Clin Biochem* 30:63–67
45. Ronco P, Brunisholz M, Geniteau-Legendre M, Chatelet F, Verroust P, Richet G (1987) Physiopathologic aspects of Tamm-Horsfall protein: a phylogenetically conserved marker of the thick ascending limb of Henle's loop. *Adv Nephrol Necker Hosp* 16:231–249
46. Rose GA, Sulaiman S (1982) Tamm-Horsfall mucoproteins promote calcium oxalate crystal formation in urine: quantitative studies. *J Urol* 127:177–179
47. Rose MB (1975) Renal stone formation. The inhibitory effect of urine on calcium oxalate precipitation. *Invest Urol* 12:428–433
48. Schnierle P (1995) A simple diagnostic method for the differentiation of Tamm-Horsfall glycoproteins from healthy probands and those from recurrent calcium oxalate renal stone formers. *Experientia* 51:1068–1072
49. Schnierle P, Hering F, Seiler H (1996) Isoelectric focusing of Tamm-Horsfall glycoproteins: a simple tool for recognizing recurrent calcium oxalate renal stone formers. *Urol Res* 24:79–82
50. Scurr DS, Robertson WG (1986) Modifiers of calcium oxalate crystallization found in urine. III. Studies on the role of Tamm-Horsfall mucoprotein and of ionic strength. *J Urol* 136:505–507
51. Serafini-Cessi F, Bellabarba G, Malagolini N, Dall'Olio F (1989) Rapid isolation of Tamm-Horsfall glycoprotein (uromodulin) from human urine. *J Immunol Methods* 120:185–189
52. Serafini-Cessi F, Monti A, Cavallone D (2005) N-Glycans carried by Tamm-Horsfall glycoprotein have a crucial role in the defense against urinary tract diseases. *Glycoconj J* 22:383–394
53. Sheng X, Jung T, Wesson JA, Ward MD (2005) Adhesion at calcium oxalate crystal surfaces and the effect of urinary constituents. *Proc Natl Acad Sci USA* 102:267–272
54. Sheng X, Ward MD, Wesson JA (2005) Crystal surface adhesion explains the pathological activity of calcium oxalate hydrates in kidney stone formation. *J Am Soc Nephrol* 16:1904–1908
55. Stevenson FK, Cleave AJ, Kent PW (1971) The effect of ions on the viscometric and ultracentrifugal behaviour of Tamm-Horsfall glycoprotein. *Biochim Biophys Acta* 236:59–66
56. Sumitra K, Pragasam V, Sakthivel R, Kalaiselvi P, Varalakshmi P (2005) Beneficial effect of vitamin E supplementation on the biochemical and kinetic properties of Tamm-Horsfall glycoprotein in hypertensive and hyperoxaluric patients. *Nephrol Dial Transplant* 20:1407–1415
57. Trewick AL, Rumsby G (1999) Isoelectric focusing of native urinary uromodulin (Tamm-Horsfall protein) shows no physicochemical differences between stone formers and non-stone formers. *Urol Res* 27:250–254
58. UniProt (2008) The universal protein resource (UniProt). *Nucleic Acids Res* 36:D190–D195
59. van Aswegen CH, van der Merwe CA, du Plessis DJ (1990) Sialic acid concentrations in the urine of men with and without renal stones. *Urol Res* 18:29–33
60. van Rooijen JJ, Voskamp AF, Kamerling JP, Vliegenthart JF (1999) Glycosylation sites and site-specific glycosylation in human Tamm-Horsfall glycoprotein. *Glycobiology* 9:21–30
61. Verkoelen CF, Van Der Boom BG, Kok DJ, Romijn JC (2000) Sialic acid and crystal binding. *Kidney Int* 57:1072–1082
62. Webber D, Radcliffe CM, Royle L, Tobiasen G, Merry AH, Rodgers AL, Sturrock ED, Wormald MR, Harvey DJ, Dwek RA, Rudd PM (2006) Sialylation of urinary prothrombin fragment 1 is implicated as a contributory factor in the risk of calcium oxalate kidney stone formation. *FEBS J* 273:3024–3037
63. Wesson JA, Ganne V, Beshensky AM, Kleinman JG (2005) Regulation by macromolecules of calcium oxalate crystal aggregation in stone formers. *Urol Res* 33:206–212
64. Wesson JA, Ward MD (2007) Pathological Biomineralization of Kidney Stones. *Elements* 3:415–421
65. Wiggins RC (1987) Uromucoid (Tamm-Horsfall glycoprotein) forms different polymeric arrangements on a filter surface under different physicochemical conditions. *Clin Chim Acta* 162:329–340
66. Williams J, Marshall RD, van HH, Vliegenthart JF (1984) Structural analysis of the carbohydrate moieties of human Tamm-Horsfall glycoprotein. *Carbohydr Res* 134:141–155